ACS APPLIED MATERIALS & INTERFACES

www.acsami.org

Research Article

Incorporating Fullerenes in Nanoscale Metal–Organic Matrixes: An Ultrasensitive Platform for Impedimetric Aptasensing of Tobramycin

Han-Wen Zhang,[§] Hong-Kai Li,[§] Zhang-Ye Han, Rongrong Yuan, and Hongming He*

Cite This: *ACS Appl. Mater. Interfaces* 2022, 14, 7350–7357

Read Online

ACCESS | Metrics & More | Article Recommendations | Supporting Information

ABSTRACT: The rational design and preparation of available fullerene@metal–organic matrix hybrid materials are of profound significance in electrochemical biosensing applications due to their unique photoelectric properties. In this work, C_{60}@UiO-66-NH_2 nanocomposites serve as greatly promising materials to modify electrodes and fix aptamers, resulting in a remarkable electrochemical aptasensor for impedimetric sensing of tobramycin (TOB). Nanoscale composites have preferable electroactivity and small particle size with more exposed functional sites, such as Zr(IV) and $-NH_2$, to immobilize aptamers for enhanced detection performance. As we know, most of the electrochemical impedance aptasensors require a long time to complete the detection process, but this prepared biosensor shows the rapid quantitative identification of target TOB within 4 min. This work expands the synthesis of functional fullerene@metal–organic matrix hybrid materials in electrochemical biosensing applications.

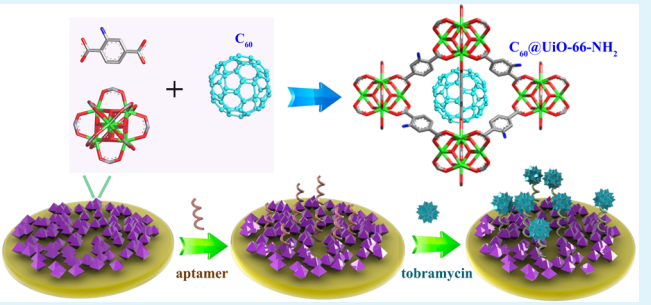

KEYWORDS: *fullerene, metal–organic framework, hybrid material, electrochemical aptasensor, tobramycin*

INTRODUCTION

In terms of achieving functional materials with task-specific functionality, the development of composite materials has drawn attention via assembling various constituents at atomic and molecular levels. Metal–organic frameworks (MOFs) have well-developed porosity, ordered structures, and various morphologies,[1] resulting in their extensive utilization in sorption,[2,3] sensor,[4−6] and heterogeneous catalysis.[7−9] Unfortunately, the poor electrochemical activity and stability of MOFs significantly limit their use in electrochemical analysis. Hence, various materials have been implemented to combine with MOFs for enhanced electrochemical activity, such as metal nanoparticles,[10] graphene,[11,12] and carbon nanotubes.[13] Notably, C_{60} is a promising candidate to assemble with MOFs for achieving available fullerene@metal–organic matrix hybrid materials. To date, only a few examples have been reported to prepare such hybrid materials,[14−20] but no C_{60}@MOF composite has been used in electrochemical detection. Therefore, it is urgently needed to develop and explore novel fullerene@metal–organic matrix species for electrochemical sensing analytes in food safety and environmental protection.

Electrochemical biosensors based on aptamers are the most extensive and useful detection method due to the sensitive and quick response of electrochemical signals and the highly specific recognition of aptamers.[21−28] Recently, many advanced materials have been developed for enhanced electrochemical detection performance, such as carbon quantum dots,[29,30] metal nanoparticles,[31,32] porous organic polymers,[33,34] and carbon nanomaterials.[35,36] Especially, Zr-based MOFs have been utilized as functional materials to prepare electrochemical aptasensors due to the superior affinity between Zr(IV) chelating sites and phosphate groups of aptamers.[37−42] Meanwhile, nanoscale particles can explore more functional sites in the outer surface to increase the interaction between MOFs and aptamers for fabricating highly sensitive aptasensors. On the other hand, several C_{60} nanohybrid-based electrochemical aptasensors have been reported to detect analytes on account of their excellent stability and electrochemical activity.[43−46] Although no electrochemical aptasensor based on C_{60}@Zr-MOF hybrid materials has been reported, previous studies indicate that such hybrid materials have great applicability in electrochemical aptasensing applications.

According to the above considerations, we first develop an available strategy to construct C_{60}@UiO-66-NH_2 nanocomposites by incorporating isolated C_{60} molecules into the internal pores of nanoscale MOFs (Scheme 1). Tobramycin (TOB) is a widely used antibiotic for treating bacterial infections, and thus, detection and analysis of TOB have

Received: December 2, 2021
Accepted: January 17, 2022
Published: January 25, 2022

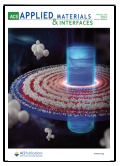

Scheme 1. Preparation and Biosensing Process of C_{60}@UiO-66-NH_2 and Its Aptasensor

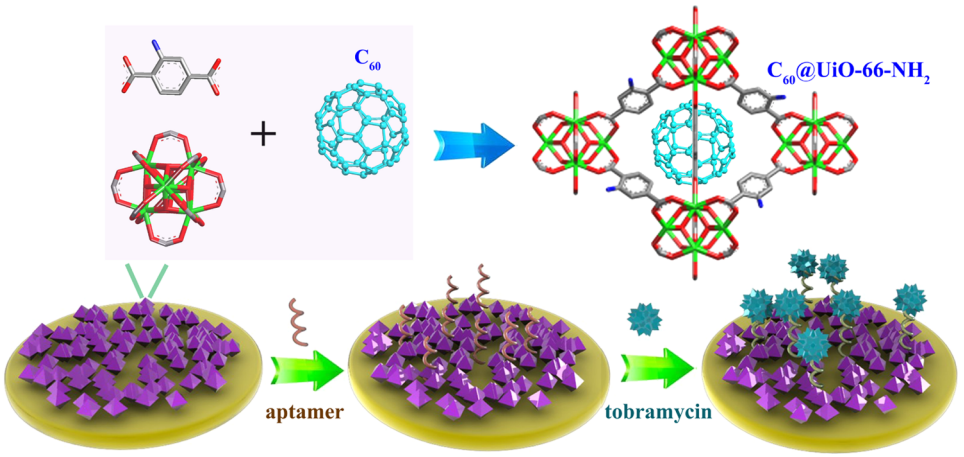

immediate practical significance.[47,48] MOF nanoparticles provide more Zr(IV) sites to coordinate with phosphate groups for increased immobilization of aptamers and amplified detection signals. Meanwhile, electroactive C_{60} with small size can be incorporated into porous skeletons to obtain nanoscale hybrid materials for improving the electrical activity of pristine MOFs. Exhilaratingly, this prepared aptasensor shows the ultrasensitive impedimetric detection of TOB. This work expands the preparation of novel hybrid materials for available electrochemical aptasensors.

EXPERIMENTAL SECTION

Synthetic Processes. Similar to previously reported nanoscale Zr-MOFs,[49] $ZrOCl_2 \cdot 8H_2O$ (21 mg) and the organic ligand 2-aminoterephthalic acid (43 mg) were severally dissolved in 3 mL and 1 mL of *N*, *N*-dimethylformamide. Both solutions were mixed and further added 500 μL of acetic acid (6 mol·L^{-1}). Nanoscale UiO-66-NH_2 samples were generated after heating at 90 °C for 19 h. Nanoparticles were centrifugally collected at 12 000 rpm for 20 min and purified by washing with 5 mL of fresh *N*,*N*-dimethylformamide, methanol, and water, successively. Similar to nanoscale UiO-66-NH_2 except adding C_{60} (3 mg), C_{60}@UiO-66-NH_2 was acquired after washing with toluene as the eluent. Toluene can dissolve and remove the freely dispersed C_{60} until the eluent is colorless.

Electrochemical Aptasensors. Aluminum powder with a particle size of 0.3 μm was used to clean the Au electrode (AE) surface, which was drenched in a mixed solution of H_2O_2 (14 mL) and H_2SO_4 (6 mL). Bare AEs were obtained after rinsing with distilled water (10 mL) and ethanol (10 mL). Material/AE was obtained by adding the ethanol dispersion (2.0 μL, 0.5 mg·mL^{-1}) on AE. After that, the apt/material/AE aptasensor was acquired after immersing material/AE in a 0.001 ng·mL^{-1} aptamer solution for 4 min, which can detect TOB via soaking in the corresponding solution for 4 min at room temperature to collect electrochemical response signals.

RESULTS AND DISCUSSION

C_{60}@UiO-66-NH_2 was synthesized via the in situ synthetic method in the presence of C_{60}. Toluene was used to wash the obtained solid materials for removing the individual C_{60} outside composites. The target sample was obtained as dark red powders until the eluent is colorless (Figures S1). Powder X-ray diffraction (PXRD) shows that they have similar main peaks and crystal planes at 7.3° (111), 8.5° (200), and 25.7° (600) (Figure 1a). Nevertheless, the absence of novel diffraction peaks in C_{60}@UiO-66-NH_2 proves that the encapsulated C_{60} has no obvious effect on the crystal texture of MOF matrixes. Meanwhile, the broader diffraction peaks of the as-synthesized samples are mainly caused by the nanosized crystal particles. Fourier transform infrared (FT-IR) spectra exhibit that this composite not only has the characteristic bands of UiO-66-NH_2 at 658, 767, 965, 1253, 1384, 1440, 1571, 1658, 3365, and 3474 cm^{-1} but also possesses three characteristic peaks at 527, 576, and 1183 cm^{-1}, which are ascribed to the C_{60} molecule incorporated in MOFs (Figure 1b).[50,51] UiO-66-NH_2 nanoparticles have Brunauer–Emmett–Teller (BET) and Langmuir surface areas of 430 and 604 $m^2 \cdot g^{-1}$, respectively, but the C_{60}@UiO-66-NH_2 nanocomposite material exhibits relatively lower BET and Langmuir surface areas of 277 and 384 $m^2 \cdot g^{-1}$, respectively, with a smaller pore volume because of nonporous C_{60} molecules encapsulated in porous MOFs (Figures 1c, S2, and S3 and Table S1). Also, Figure 1d demonstrates that the pore size of the pristine MOF is evidently larger than the composite because the MOF skeleton has larger pore sizes at ~7.3 and ~12.7 Å than the molecular size of C_{60} (7.1 Å) to capture C_{60} molecules.[52] Nevertheless, the preservation of N_2 sorption capacity and pore size distribution exhibit that only a part of pores is filled with C_{60} molecules. Due to the randomness of C_{60} molecules embedded in UiO-66-NH_2, it is difficult to accurately determine the number of C_{60} molecules in one single pore of the MOF. A pore size of ~7.3 Å can constraint one C_{60} molecule and the other large pore (~12.7 Å) may incorporate 1–2 C_{60} molecules. Moreover, the encapsulation amount of C_{60} in C_{60}@UiO-66-NH_2 is calculated to be ~7% via elemental analysis, which is similar to the result of thermogravimetric analysis (TGA) in air (Figures S4 and S5). A methanol suspension of the C_{60}@UiO-66-NH_2 composite (1 mg·mL^{-1}) was used to prepare test samples before scanning and transmission electron microscopies (SEM and TEM). As shown in Figures 1e–f and S6, this composite consists of nanoscale particles with grain diameters from 15 to 30 nm.

The Randles equivalent circuit is used to analyze electrochemical impedance spectroscopy (EIS) data (Figure S7). To obtain the most effective detectability, the optimal experimental conditions of aptasensors were explored through analyzing the test R_{ct} value, such as the addition amount of the composite and the incubation time in an aptamer solution. As shown in Figure 2a, the variation of the R_{ct} value (ΔR_{ct} = $R_{ct,\ C60@UiO-66-NH2/AE} - R_{ct,\ AE}$) enhances gradually with the increase of the addition quantity of C_{60}@UiO-66-NH_2. The most appropriate amount is 2 μg of the hybrid material. The ΔR_{ct} value increases with the extension of the incubation time

https://doi.org/10.1021/acsami.1c23320
ACS Appl. Mater. Interfaces 2022, 14, 7350–7357

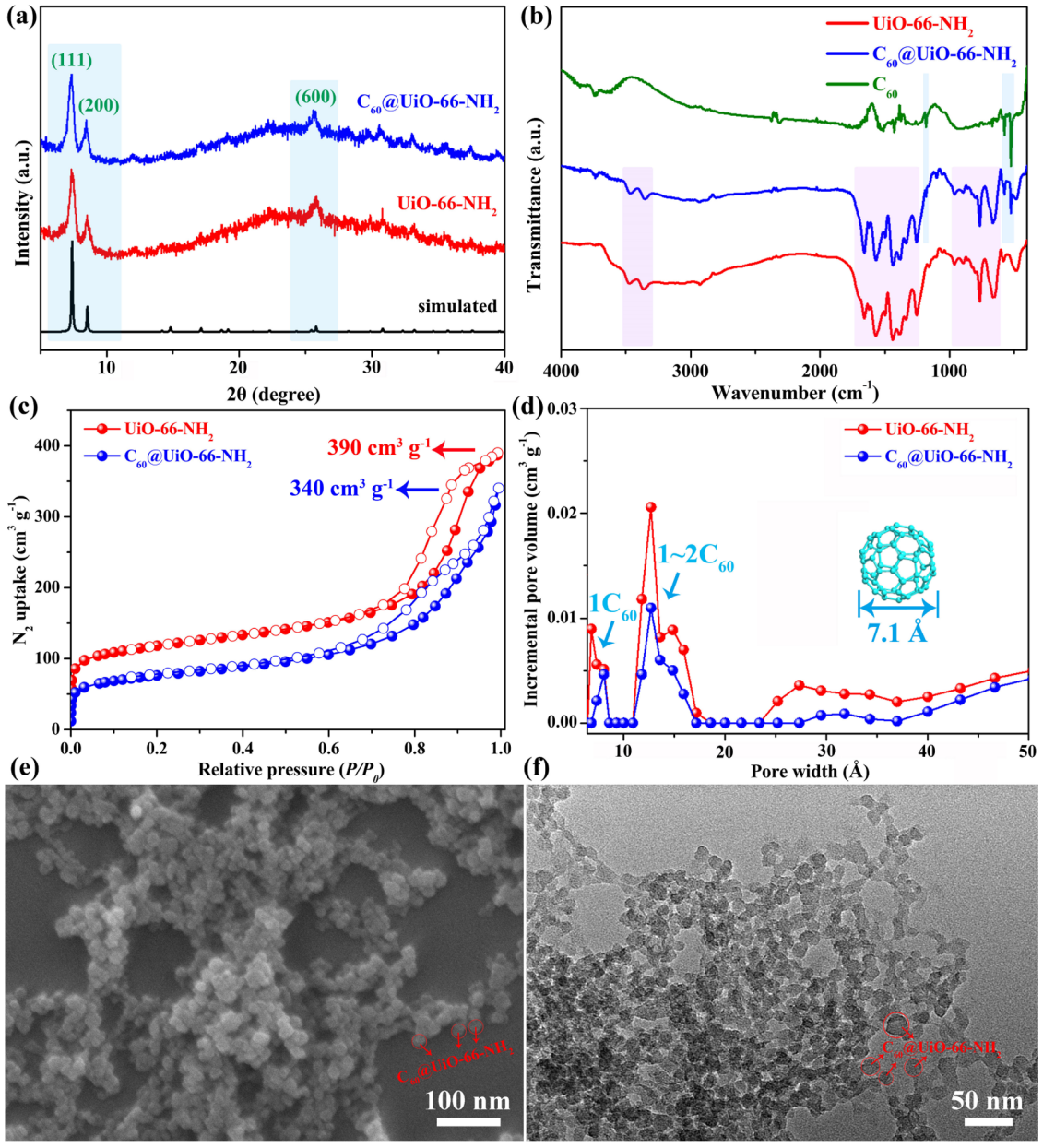

Figure 1. Structural characterization: (a) PXRD, (b) FT-IR, (c) N_2 curve, and (d) inner porosity distribution. The morphology of C_{60}@UiO-66-NH_2 observed by (e) SEM and (f) TEM.

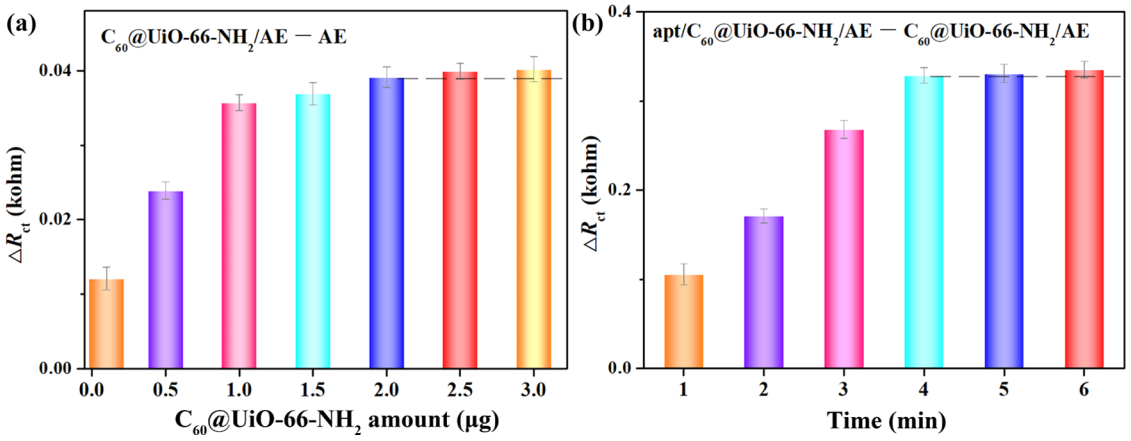

Figure 2. Optimal preparation conditions: (a) C_{60}@UiO-66-NH_2 amount and (b) incubation time in an aptamer solution.

https://doi.org/10.1021/acsami.1c23320
ACS Appl. Mater. Interfaces 2022, 14, 7350−7357

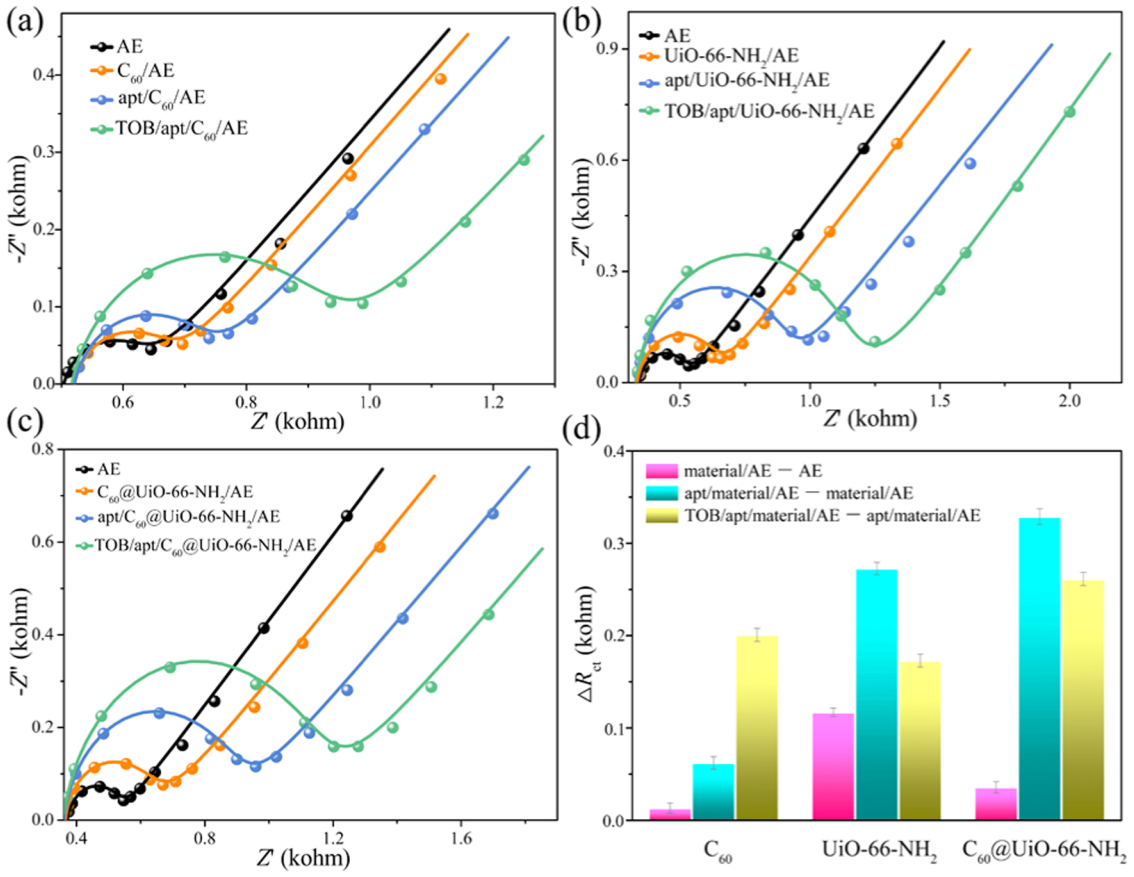

Figure 3. (a–c) EIS data of these aptasensors and (d) comparison of different material-modified AEs at each stage.

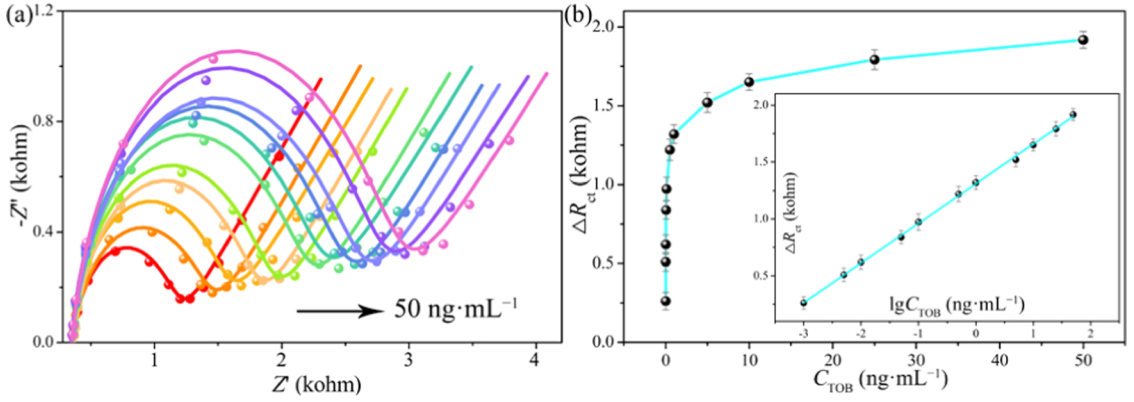

Figure 4. (a) EIS data of this aptasensor after soaking in TOB solutions at different concentrations. (b) The nonlinear relationship of ΔR_{ct} and TOB concentration (inset: the linearity of ΔR_{ct} and the logarithm of the TOB concentration).

in a 0.001 ng·mL^{-1} aptamer solution. It confirms that the optimal soaking time is 4 min to immobilize aptamers to create an aptasensor (Figure 2b), which is obviously shorter than most reported aptasensors.[11,21,33,34,37]

The EIS Nyquist plots of these prepared aptasensors based on various materials have similar electrochemical impedimetric behaviors during the fabricating process. As displayed in Figure 3a–c, the semicircles of the EIS Nyquist plots evidently enlarge with additive layers on AEs, including the functional material, aptamer, and TOB, because these organic layers have relatively poor electroconductibility to obstruct the electron transport.[53] Notably, C_{60}@UiO-66-NH_2 can fabricate a more efficient electrochemical aptasensor due to electroactive C_{60} and nanoscale MOFs with high surface areas, abound Zr(IV) sites, large conjugated π system, and excellent stability (Figure 3d). The EIS Nyquist plots of AE have the smallest semicircle with an R_{ct} value of 0.159 kohm because of fine electrical conductivity and a clean electrode surface. The R_{ct} value increases to 0.195 kohm after adding C_{60}@UiO-66-NH_2 on AEs (denoted C_{60}@UiO-66-NH_2/AE), which further enhances as high as 0.524 kohm after immersing in an aptamer solution (0.001 ng·mL^{-1}) for acquiring the aptasensor (denoted apt/C_{60}@UiO-66-NH_2/AE). The fabricated aptasensor exhibits a significantly higher R_{ct} value after soaking in the TOB aqueous solution for 4 min at 0.001 ng·mL^{-1} (denoted TOB/C_{60}@UiO-66-NH_2/AE), which clearly indicates that this biosensor

https://doi.org/10.1021/acsami.1c23320
ACS Appl. Mater. Interfaces 2022, 14, 7350−7357

Table 1. Sensing Performance of Different Test Methods and Functional Materials

material	test method	time (min)	linear concentration range ($nmol·L^{-1}$)	LOD ($nmol·L^{-1}$)	ref
Au NPs	UV−vis spectroscopy	15	40−200	23.3	54
Au NPs	resonance scattering spectroscopy	15	0.5−17	0.19	55
SnO_2/Bi_2S_3	photoelectrochemistry	120	5−50	4.28	56
molecular-imprinted polypyrrole	square wave voltammetry		0.5−10	0.14	57
Au NPs	UV−vis spectroscopy		43−380	1.2	58
MoS_x@ZnO core−shell nanorod	photoelectrochemistry	60	2.1×10^{2}−106.9	0.012	59
C_{60}@UiO-66-NH_2	electrochemical impedance spectroscopy	4	2.1×10^{3}−106.9	0.377 $pmol·L^{-1}$	this work

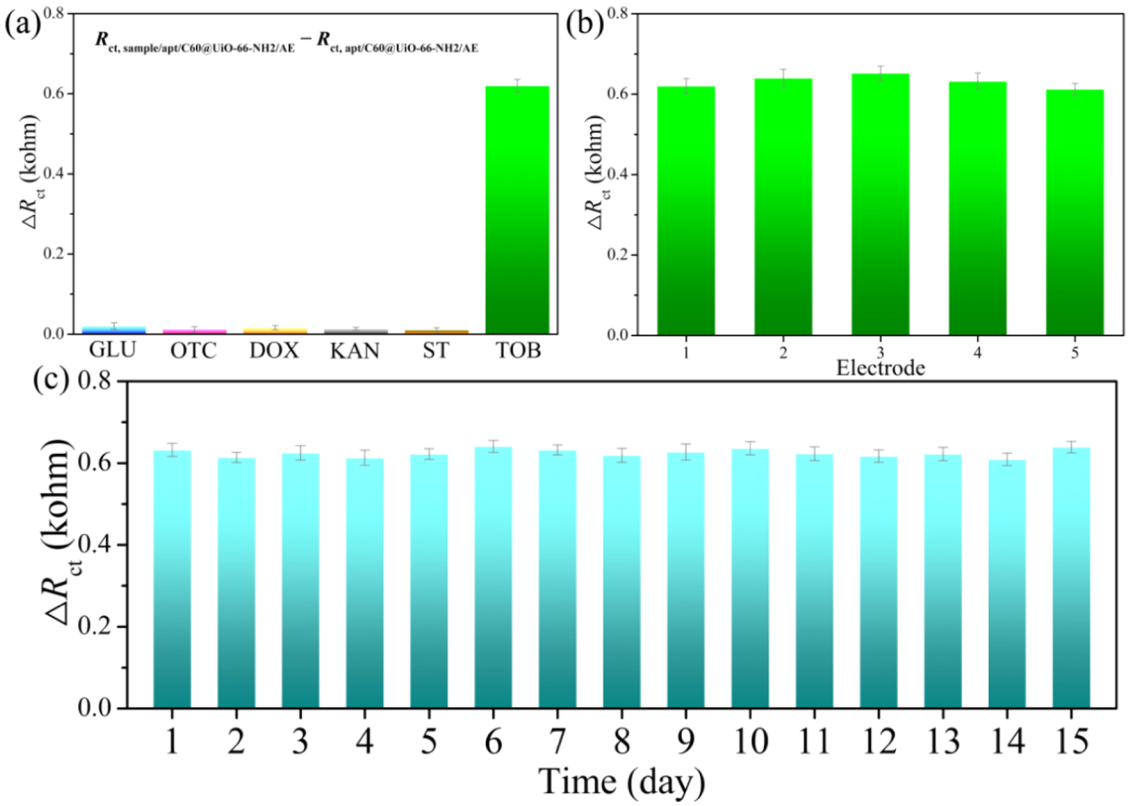

Figure 5. Sensing performance of aptasensor: (a) selectivity, (b) reproducibility, and (c) stability.

can sensitively detect ultratrace TOB via EIS Nyquist plots. Additionally, simple mixed materials of UiO-66-NH_2 (93 wt %) and different carbon materials (7 wt %), including C_{60}, carbon nanotubes, and graphene, were prepared to construct different electrochemical aptasensors. As shown in Figures S8−S11, these material-modified AEs have obviously different ΔR_{ct} values ($\Delta R_{ct} = R_{ct,\ apt/material/AE} - R_{ct,\ material/AE}$) in a 0.001 ng·$mL^{-1}$ aptamer solution, which are all smaller than that of the hybrid material-based aptasensor. C_{60}@UiO-66-NH_2 is constructed via C_{60} as a guest molecule embedded in UiO-66-NH_2, which has no effect on the interaction between the Zr(IV) site and the aptamer. Compared with physically mixed hybrid materials, the high immobilization of the aptamer on C_{60}@UiO-66-NH_2 is mainly caused by more Zr(IV) sites of C_{60}@UiO-66-NH_2 than those of C_{60}, carbon nanotubes, or graphene/UiO-66-NH_2. Hence, the composite material exhibits the highest ΔR_{ct} value ($\Delta R_{ct} = R_{ct,\ TOB/apt/material/AE} - R_{ct,\ apt/material/AE}$) among these fabricated aptasensors for detecting TOB (0.001 ng·mL^{-1}), confirming that this composite is a good functional material for constructing a sensitive electrochemical aptasensor.

In addition, the electrochemical biosensor was separately soaked in TOB solutions at 0.001, 0.005, 0.01, 0.05, 0.1, 0.5, 1.0, 5.0, 10.0, 25.0, and 50.0 ng·mL^{-1} for 4 min to measure EIS Nyquist plots. As the TOB concentration increases, the R_{ct} value gradually enhances because of the generation of more TOB/aptamer complexes to effectively hinder electron transfer (Figure 4a). The ΔR_{ct} value is calculated to analyze the sensing ability of this aptasensor toward TOB. As shown in Figure 4b, ΔR_{ct} value and TOB concentration show an obvious nonlinear relation, but the ΔR_{ct} value shows a linear relation with the logarithm of the TOB concentration (0.001−50.0 ng·mL^{-1}) as $\Delta R_{ct} = 0.3487 \times \lg C_{TOB} + 1.309$ with a correlation coefficient of 0.9993. The aptasensor shows a remarkable detection performance toward TOB with a limit of detection (LOD) of ~0.176 pg·mL^{-1} (~0.377 $pmol·L^{-1}$) by comparing it with some previously reported materials and test methods (Table 1).[54−59] By referring to earlier literature studies,[37−42,60] the prepared UiO-66-NH_2 nanoparticles not only have abound Zr(IV) sites to immobilize aptamers via the coordination interaction but also possess various functional sites, such as $-NH_2$ and conjugate skeleton, to interact with the biological

https://doi.org/10.1021/acsami.1c23320
ACS Appl. Mater. Interfaces 2022, 14, 7350−7357

base of aptamers. Subsequently, the fixed aptamers have a specific affinity force toward the target TOB molecule, resulting in the highly selective and sensitive sensing performance. The accurate detection mechanism, however, is still uncertain, which requires many advanced equipment to further investigate the authentic structure−response relationship.

Other aptasensing properties were evaluated in detail via the ΔR_{ct} value. First, this electrochemical aptasensor was soaked in TOB or other interferences at 10 pg·mL^{-1} such as doxycycline (DOX), glucose (GLU), kanamycin (KAN), streptomycin sulfate (ST), and oxytetracycline (OTC). The ΔR_{ct} value was collected to compare with each other for evaluating the selectivity of this aptasensor. As displayed in Figure 5a, the ΔR_{ct} values are negligible after soaking in these interferences, but a significantly increased ΔR_{ct} value is observed in a TOB solution because of the high specificity of the aptamer. Then, five aptasensors were parallelly prepared to monitor TOB at 10 pg·mL^{-1}. These prepared aptasensors have similar ΔR_{ct} values with relative standard deviation (RSD) under 4.29% (Figure 5b). Moreover, this fabricated electrochemical aptasensor can retain the sensing performance toward TOB (10 pg·mL^{-1}) for 15 days in a refrigerator at −20 °C with similar ΔR_{ct} values (Figure 5c). Hence, these results demonstrate the excellent superior sensing performance of this aptasensor toward TOB. The quantitative analysis of TOB in various real samples was performed using this aptasensor. EIS Nyquist plots were acquired after immersing in these samples at 0.1, 1.0, and 10.0 ng·mL^{-1}, which were separately analyzed via the linear regression equation. The detectable TOB concentrations are matched well with those of really added amounts (Table 2).

Table 2. Detection of TOB in Human Serum, Urine, and Saliva

samples	added amount (ng·mL^{-1})	detected amount (ng·mL^{-1})	recovery (%)	RSD (%)
human serum	0.1	0.0981	98.1	3.07
	1.0	1.027	102.7	3.51
	10.0	10.41	104.1	3.92
urine	0.1	0.0987	98.7	2.94
	1.0	1.033	103.3	3.77
	10.0	10.37	103.7	3.81
saliva	0.1	0.1039	103.9	2.98
	1.0	1.048	104.8	4.07
	10.0	9.86	98.6	3.01

Furthermore, the recoveries of this aptasensor toward TOB are in the range of 98.1−104.8% with RSD values under 4.07%. The sensing performance illustrates the available detectability of this aptasensor in real samples.

CONCLUSIONS

Herein, C_{60}@UiO-66-NH_2 hybrid materials with particle sizes from 15 to 30 nm are first prepared to fabricate electrochemical aptasensors. The impedance aptasensor not only exhibits more sensitive sensing performance toward TOB than other physically mixed carbon material/UiO-66-NH_2 nanohybrids but also realizes the fast quantitative detection of trace TOB even in real samples within 4 min. This work shows a feasible approach for the design and synthesis of functional composites and their electrochemical aptasnesors.

ASSOCIATED CONTENT

Supporting Information

The Supporting Information is available free of charge at https://pubs.acs.org/doi/10.1021/acsami.1c23320.

IBET surface area plots; TGA; EIS; and so on (PDF)

AUTHOR INFORMATION

Corresponding Author

Hongming He − *Tianjin Key Laboratory of Structure and Performance for Functional Molecules, College of Chemistry, Tianjin Normal University, Tianjin 300387, China;* orcid.org/0000-0001-5535-8825; Email: hehongminghz@163.com, hxxyhhm@tjnu.edu.cn

Authors

Han-Wen Zhang − *Tianjin Key Laboratory of Structure and Performance for Functional Molecules, College of Chemistry, Tianjin Normal University, Tianjin 300387, China*

Hong-Kai Li − *Tianjin Key Laboratory of Structure and Performance for Functional Molecules, College of Chemistry, Tianjin Normal University, Tianjin 300387, China*

Zhang-Ye Han − *Tianjin Key Laboratory of Structure and Performance for Functional Molecules, College of Chemistry, Tianjin Normal University, Tianjin 300387, China*

Rongrong Yuan − *Department of Materials Science and Engineering, Jilin Jianzhu University, Changchun 130118, China*

Complete contact information is available at: https://pubs.acs.org/10.1021/acsami.1c23320

Author Contributions

[§]H.-W.Z. and H.-K.L. contributed equally.

Notes

The authors declare no competing financial interest.

ACKNOWLEDGMENTS

The authors thank the National Natural Science Foundation of China (21801187) and the Opening Project of Key Laboratory of Polyoxometalate and Reticular Material Chemistry of Ministry of Education for fund support.

REFERENCES

(1) "Joe" Zhou, H. C.; Kitagawa, S. Metal−Organic Frameworks (MOFs). *Chem. Soc. Rev.* **2014**, *43*, 5415−5418.

(2) Chapman, E.; Ullah, S.; Wang, H.; Feng, L.; Wang, K.; Zhou, H.-C.; Li, J.; Thonhauser, T.; Tan, K. Tuning the Adsorption Properties of Metal−Organic Frameworks through Coadsorbed Ammonia. *ACS Appl. Mater. Interfaces* **2021**, *13*, 43661−43667.

(3) Zhou, P.; Yue, L.; Wang, X.; Fan, L.; Chen, D.-L.; He, Y. Improving Ethane/Ethylene Separation Performance of Isoreticular Metal−Organic Frameworks via Substituent Engineering. *ACS Appl. Mater. Interfaces* **2021**, *13*, 54059−54068.

(4) Yuan, R.; He, H. State of the Art Methods and Challenges of Luminescent Metal−Organic Frameworks for Antibiotic Detection. *Inorg. Chem. Front.* **2020**, *7*, 4293−4319.

(5) He, H.; Zhu, Q.-Q.; Li, C.-P.; Du, M. Design of a Highly-Stable Pillar-Layer Zinc(II) Porous Framework for Rapid, Reversible, and Multi-Responsive Luminescent Sensor in Water. *Cryst. Growth Des.* **2019**, *19*, 694−703.

(6) Han, L.-J.; Kong, Y.-J.; Zhang, X.-M.; Hou, G.-Z.; Chen, H.-C.; Zheng, H.-G. Fluorescence Recognition of Adenosine Triphosphate and Uric Acid by Two Eu-Based Metal−Organic Frameworks. *J. Mater. Chem. C* **2021**, *9*, 6051−6061.

(7) Wang, S.; Zhang, X.; Chang, X.; Zong, M.-Y.; Fan, C.-Z.; Guo, D.-X.; Xu, J.; Wang, D.-H.; Bu, X.-H. Rational Design of Ionic V-MOF with Confined Mo Species for Highly Efficient Oxidative Desulfurization. *Appl. Catal., B* **2021**, *298*, No. 120594.
(8) He, H.; Zhu, Q.-Q.; Yan, Y.; Zhang, H.-W.; Han, Z.-Y.; Sun, H.; Chen, J.; Li, C.-P.; Zhang, Z.; Du, M. Metal−Organic Framework Supported Au Nanoparticles with Organosilicone Coating for High-Efficiency Electrocatalytic N2 Reduction to NH3. *Appl. Catal., B* **2022**, *302*, No. 120840.
(9) He, H.; Sun, Q.; Gao, W.; Perman, J. A.; Sun, F.; Zhu, G.; Aguila, B.; Forrest, K.; Space, B.; Ma, S. A Stable Metal−Organic Framework Featuring Local Buffer Environment for Carbon Dioxide Fixation. *Angew. Chem., Int. Ed.* **2018**, *57*, 4657−4662.
(10) Yang, Y.; Yang, Z.; Lv, J.; Yuan, R.; Chai, Y. Thrombin Aptasensor Enabled by Pt Nanoparticles-Functionalized Co-Based Metal Organic Frameworks Assisted Electrochemical Signal Amplification. *Talanta* **2017**, *169*, 44−49.
(11) Zhu, Q.-Q.; Zhang, H.-W.; Yuan, R.; He, H. Ingenious Fabrication of Metal−Organic Framework/Graphene Oxide Composites as Aptasensors with Superior Electrochemical Recognition Capability. *J. Mater. Chem. C* **2020**, *8*, 15823−15829.
(12) Zhang, S.; Liu, L.; Yang, J.; Zhang, Y.; Wan, Z.; Zhou, L. Pd-Ru-Bi Nanoalloys Modified Three-Dimensional Reduced Graphene Oxide/MOF-199 Composites as a Highly Efficient Electrocatalyst for Ethylene Glycol Electrooxidation. *Appl. Surf. Sci.* **2019**, *492*, 617−625.
(13) Shen, C.-H.; Chuang, C.-H.; Gu, Y.-J.; Ho, W. H.; Song, Y.-D.; Chen, Y.-C.; Wang, Y.-C.; Kung, C.-W. Cerium-Based Metal−Organic Framework Nanocrystals Interconnected by Carbon Nanotubes for Boosting Electrochemical Capacitor Performance. *ACS Appl. Mater. Interfaces* **2021**, *13*, 16418−16426.
(14) Pratik, S. M.; Gagliardi, L.; Cramer, C. J. Engineering Electrical Conductivity in Stable Zirconium-Based PCN-222 MOFs with Permanent Mesoporosity. *Chem. Mater.* **2020**, *32*, 6137−6149.
(15) Ohmura, T.; Usuki, A.; Mukae, Y.; Motegi, H.; Kajiya, S.; Yamamoto, M.; Senda, S.; Matsumoto, T.; Tatsumi, K. Supramolecular Porphyrin-Based Metal−Organic Frameworks with Fullerenes: Crystal Structures and Preferential Intercalation of C70. *Chem. - Asian J.* **2016**, *11*, 700−704.
(16) Li, H.; Hill, M. R.; Huang, R.; Doblin, C.; Lim, S.; Hill, A. J.; Babarao, R.; Falcaro, P. Facile Stabilization of Cyclodextrin Metal−Organic Frameworks under Aqueous Conditions via the Incorporation of C60 in Their Matrices. *Chem. Commun.* **2016**, *52*, 5973−5976.
(17) Saura-Sanmartin, A.; Martinez-Cuezva, A.; Marin-Luna, M.; Bautista, D.; Berna, J. Effective Encapsulation of C60 by Metal−Organic Frameworks with Polyamide Macrocyclic Linkers. *Angew. Chem.* **2021**, *133*, 10909−10914.
(18) Souto, M.; Calbo, J.; Mañas-Valero, S.; Walsh, A.; Espallargas, G. M. Charge-Transfer Interactions Between Fullerenes and a Meso-Porous Tetrathiafulvalene-Based Metal−Organic Framework. *Beilstein J. Nanotechnol.* **2019**, *10*, 1883−1893.
(19) Martinez, V.; Karadeniz, B.; Biliškov, N.; Loncari, I.; Muratovic, S.; Zilic, D.; Avdoshenko, S. M.; Roslova, M.; Popov, A. A.; Uzarevic, K. Tunable Fulleretic Sodalite MOFs: Highly Efficient and Controllable Entrapment of C60 Fullerene via Mechanochemistry. *Chem. Mater.* **2020**, *32*, 10628−10640.
(20) Zuo, J.; Yuan, Y.; Zhao, M.; Wang, J.; Chen, Y.; Zhu, Q.; Bai, L. An Efficient Electrochemical Assay for miR-3675-3p in Human Serum Based on the Nanohybrid of Functionalized Fullerene and Metal−Organic Framework. *Anal. Chim. Acta* **2020**, *1140*, 78−88.
(21) Zhu, Q.-Q.; Zhang, W.-W.; Zhang, H.-W.; Yuan, R.; He, H. Elaborately Manufacturing an Electrochemical Aptasensor Based on Gold Nanoparticle/COF Composites for Amplified Detection Performance. *J. Mater. Chem. C* **2020**, *8*, 16984−16991.
(22) Li, L.; Yang, L.; Zhang, S.; Sun, Y.; Li, F.; Qin, T.; Liu, X.; Zhou, Y.; Alwarappan, S. A NiCo2S4@N/S-CeO2 Composite as an Electrocatalytic Signal Amplification Label for Aptasensing. *J. Mater. Chem. C* **2020**, *8*, 14723−14731.
(23) Li, H.-K.; Ye, H.-L.; Zhao, X.-X.; Sun, X.-L.; Zhu, Q.-Q.; Han, Z.-Y.; Yuan, R.; He, H. Artful Union of a Zirconium-Porphyrin MOF/GO Composite for Fabricating an Aptamer-Based Electrochemical Sensor with Superb Detecting Performance. *Chin. Chem. Lett.* **2021**, *32*, 2851−2855.
(24) Hu, X.; Wei, P.; Catananta, G.; Li, Z.; Marty, J. L.; Zhu, Z. Ultrasensitive Ciprofloxacin Assay Based on the Use of a Fluorescently Labeled Aptamer and a Nanocomposite Prepared from Carbon Nanotubes and MoSe2. *Microchimica Acta* **2019**, *186*, No. 507.
(25) Hu, X.; Goud, K. Y.; Kumar, V. S.; Catanante, G.; Li, Z.; Zhu, Z.; Marty, J. L. Disposable Electrochemical Aptasensor Based on Carbon Nanotubes-V2O5-Chitosan Nanocomposite for Detection of Ciprofloxacin. *Sens. Actuators, B* **2018**, *268*, 278−286.
(26) Ming, T.; Cheng, Y.; Xing, Y.; Luo, J.; Mao, G.; Liu, J.; Sun, S.; Kong, F.; Jin, H.; Cai, X. Electrochemical Microfluidic Paper-Based Aptasensor Platform Based on a Biotin−Streptavidin System for Label-Free Detection of Biomarkers. *ACS Appl. Mater. Interfaces* **2021**, *13*, 46317−46324.
(27) Wang, S.; He, B.; Liang, Y.; Jin, H.; Wei, M.; Ren, W.; Suo, Z.; Wang, J. Exonuclease III-Driven Dual-Amplified Electrochemical Aptasensor Based on PDDA-Gr/PtPd@Ni-Co Hollow Nanoboxes for Chloramphenicol Detection. *ACS Appl. Mater. Interfaces* **2021**, *13*, 26362−26372.
(28) He, X.; Dong, J.; Han, H.; Sun, N.; Shi, W.; Lu, X.; Jia, H.; Lu, X. A Novel Electrochemical Aptasensor for the Ultrasensitive Detection of Adenosine Triphosphate Based on DNA-Templated Copolymers. *ACS Appl. Mater. Interfaces* **2021**, *13*, 35561−35567.
(29) Eksin, E.; Senturk, H.; Zor, E.; Bingol, H.; Erdem, A. Carbon Quantum Dot Modified Electrodes Developed for Electrochemical Monitoring of Daunorubicin-DNA Interaction. *J. Electroanal. Chem.* **2020**, *862*, No. 114011.
(30) Abazar, F.; Noorbakhsh, A. Chitosan-Carbon Quantum Dots as a New Platform for Highly Sensitive Insulin Impedimetric Aptasensor. *Sens. Actuators, B* **2020**, *304*, No. 127281.
(31) Liu, Y.; Xu, Q.; Zhang, Y.; Ren, B.; Huang, L.; Cai, H.; Xu, T.; Liu, Q.; Zhang, X. An Electrochemical Aptasensor Based on AuPt Alloy Nanoparticles for Ultrasensitive Detection of Amyloid-Beta Oligomers. *Talanta* **2021**, *231*, No. 122360.
(32) Cai, H.; Zhu, N.; Jiang, Y.; He, P.; Fang, Y. Cu@Au Alloy Nanoparticle as Oligonucleotides Labels for Electrochemical Stripping Detection of DNA Hybridization. *Biosens. Bioelectron.* **2003**, *18*, 1311−1319.
(33) Yuan, R.; Yan, Z.; Shaga, A.; He, H. Design and Fabrication of an Electrochemical Sensing Platform Based on a Porous Organic Polymer for Ultrasensitive Ampicillin Detection. *Sens. Actuators, B* **2021**, *327*, No. 128949.
(34) Han, Z.-Y.; Zhu, Q.-Q.; Zhang, H.-W.; Yuan, R.; He, H. A Porous Organic Framework Composite Embedded with Au Nanoparticles: An Ultrasensitive Electrochemical Aptasensor toward Detection of Oxytetracycline. *J. Mater. Chem. C* **2020**, *8*, 14075−14082.
(35) Vasilescu, A.; Hayat, A.; Gaspar, S.; Marty, J. L. Advantages of Carbon Nanomaterials in Electrochemical Aptasensors for Food Analysis. *Electroanalysis* **2018**, *30*, 2−19.
(36) Mu, Z.; Tian, J.; Wang, J.; Zhou, J.; Bai, L. A New Electrochemical Aptasensor for Ultrasensitive Detection of Endotoxin Using Fe-MOF and AgNPs Decorated P-N-CNTs as Signal Enhanced Indicator. *Appl. Surf. Sci.* **2022**, *573*, No. 151601.
(37) Zhang, H.-W.; Zhu, Q.-Q.; Yuan, R.; He, H. Crystal Engineering of MOF@COF Core-Shell Composites for Ultra-Sensitively Electrochemical Detection. *Sens. Actuators, B* **2021**, *329*, No. 129144.
(38) Dai, G.; Li, Z.; Luo, F.; Ai, S.; Chen, B.; Wang, Q. Electrochemical Determination of Salmonella Typhimurium by Using Aptamer-Loaded Gold Nanoparticles and a Composite Prepared from a Metal−Organic Framework (Type UiO-67) and Graphene. *Microchim. Acta* **2019**, *186*, No. 620.

https://doi.org/10.1021/acsami.1c23320
ACS Appl. Mater. Interfaces 2022, 14, 7350−7357

(39) Li, N.; Huang, X.; Sun, D.; Yu, W.; Tan, W.; Luo, Z.; Chen, Z. Dual-Aptamer-Based Voltammetric Biosensor for the Mycobacterium Tuberculosis Antigen MPT64 by Using a Gold Electrode Modified with a Peroxidase Loaded Composite Consisting of Gold Nanoparticles and a Zr(IV)/Terephthalate Metal−Organic Framework. *Microchim. Acta* **2018**, *185*, No. 543.
(40) Qiu, W.; Gao, F.; Yano, N.; Kataoka, Y.; Handa, M.; Yang, W.; Tanaka, H.; Wang, Q. Specific Coordination Between Zr-MOF and Phosphate-Terminated DNA Coupled with Strand Displacement for the Construction of Reusable and Ultrasensitive Aptasensor. *Anal. Chem.* **2020**, *92*, 11332−11340.
(41) Liu, S.; Bai, J.; Huo, Y.; Ning, B.; Peng, Y.; Li, S.; Han, D.; Kang, W.; Gao, Z. A Zirconium-Porphyrin MOF-Based Ratiometric Fluorescent Biosensor for Rapid and Ultrasensitive Detection of Chloramphenicol. *Biosens. Bioelectron.* **2020**, *149*, No. 111801.
(42) He, B.; Dong, X. Hierarchically Porous Zr-MOFs Labelled Methylene Blue as Signal Tags for Electrochemical Patulin Aptasensor Based on ZnO Nano Flower. *Sens. Actuators, B* **2019**, *294*, 192−198.
(43) Han, J.; Zhuo, Y.; Chai, Y.; Yuan, R.; Xiang, Y.; Zhu, Q.; Liao, N. Multi-Labeled Functionalized C60 Nanohybrid as Tracing Tag for Ultrasensitive Electrochemical Aptasensing. *Biosens. Bioelectron.* **2013**, *46*, 74−79.
(44) Chen, Y.; Liu, X.; Guo, S.; Cao, J.; Zhou, J.; Zuo, J.; Bai, L. A Sandwich-Type Electrochemical Aptasensor for Mycobacterium Tuberculosis MPT64 Antigen Detection Using C60NPs Decorated N-CNTs/GO Nanocomposite Coupled with Conductive PEI-Functionalized Metal−Organic Framework. *Biomaterials* **2019**, *216*, No. 119253.
(45) You, H.; Bai, L.; Yuan, Y.; Zhou, J.; Bai, Y.; Mu, Z. An Amperometric Aptasensor for Ultrasensitive Detection of Sulfadimethoxine Based on Exonuclease-Assisted Target Recycling and New Signal Tracer for Amplification. *Biosens. Bioelectron.* **2018**, *117*, 706−712.
(46) Roushani, M.; Shandost-Fard, F.; Azadbakht, A. Using Au@Nano-C60 Nanocomposite as an Enhanced Sensing Platform in Modeling a TNT Aptasensor. *Anal. Biochem.* **2017**, *534*, 78−85.
(47) Liu, J.; Wagan, S.; Dávila, M. M.; Taylor, J.; White, R. J. Achieving Reproducible Performance of Electrochemical, Folding Aptamer-Based Sensors on Microelectrodes: Challenges and Prospects. *Anal. Chem.* **2014**, *86*, 11417−11424.
(48) Rowe, A. A.; Miller, E. A.; Plaxco, K. W. Reagentless Measurement of Aminoglycoside Antibiotics in Blood Serum via an Electrochemical, Ribonucleic Acid Aptamer-Based Biosensor. *Anal. Chem.* **2010**, *82*, 7090−7095.
(49) Morris, W.; Briley, W. E.; Auyeung, E.; Cabezas, M. D.; Mirkin, C. A. Nucleic Acid−Metal Organic Framework (MOF) Nanoparticle Conjugates. *J. Am. Chem. Soc.* **2014**, *136*, 7261−7264.
(50) Ţucureanu, V.; Matei, A.; Avram, A. M. FTIR Spectroscopy for Carbon Family Study. *Crit. Rev. Anal. Chem.* **2016**, *46*, 502−520.
(51) Schettino, V.; Pagliai, M.; Ciabini, L.; Cardini, G. The Vibrational Spectrum of Fullerene C60. *J. Phys. Chem. A* **2001**, *105*, 11192−11196.
(52) Yuan, Y.; Cui, P.; Tian, Y.; Zou, X.; Zhou, Y.; Sun, F.; Zhu, G. Coupling Fullerene into Porous Aromatic Frameworks for Gas Selective Sorption. *Chem. Sci.* **2016**, *7*, 3751−3756.
(53) Xue, Y.-Q.; Yang, X.; Sun, X.-L.; Han, Z.-Y.; Sun, J.; He, H. Reversible Structural Transformation of CuI−TbIII Heterometallic MOFs with Highly Efficient Detection Capability toward Penicillin. *Inorg. Chem.* **2021**, *60*, 11081−11089.
(54) Ma, Q.; Wang, Y.; Jia, J.; Xiang, Y. Colorimetric Aptasensors for Determination of Tobramycin in Milk and Chicken Eggs Based on DNA and Gold Nanoparticles. *Food Chem.* **2018**, *249*, 98−103.
(55) Yan, S.; Lai, X.; Wang, Y.; Ye, N.; Xiang, Y. Label Free Aptasensor for Ultrasensitive Detection of Tobramycin Residue in Pasteurized Cow's Milk Based on Resonance Scattering Spectra and Nanogold Catalytic Amplification. *Food Chem.* **2019**, *295*, 36−41.
(56) Liu, X.; Jiang, Y.; Luo, J.; Guo, X.; Ying, Y.; Wen, Y.; Yang, H.; Wu, Y. A SnO2/Bi2S3-Based Photoelectrochemical Aptasensor for Sensitive Detection of Tobramycin in Milk. *Food Chem.* **2021**, *344*, No. 128716.
(57) Gupta, V. K.; Yola, M. L.; Özaltın, N.; Atar, N.; Ustundag, Z.; Uzun, L. Molecular Imprinted Polypyrrole Modified Glassy Carbon Electrode for the Determination of Tobramycin. *Electrochim. Acta* **2013**, *112*, 37−43.
(58) Wang, R.; Fan, S.; Wang, R.; Wang, R.; Dou, H.; Wang, L. Determination of Aminoglycoside Antibiotics by a Colorimetric Method Based on the Aggregation of Gold Nanoparticles. *Nano* **2013**, *8*, No. 1350037.
(59) Shang, M.; Zhang, J.; Qi, H.; Gao, Y.; Yan, J.; et al. All-Electrodeposited Amorphous MoSx@ZnO Core-Shell Nanorod Arrays for Self-Powered Visible-Light-Activated Photoelectrochemical Tobramycin Aptasensing. *Biosens. Bioelectron.* **2019**, *136*, 53−59.
(60) Yuan, R.; Li, H.-K.; He, H. Recent Advances in Metal/Covalent Organic Framework-Based Electrochemical Aptasensors for Biosensing Applications. *Dalton Trans.* **2021**, *50*, 14091−14104.

https://doi.org/10.1021/acsami.1c23320
ACS Appl. Mater. Interfaces 2022, 14, 7350−7357